ANALYSIS AND REPAIR OF FLAWS IN THICK STRUCTURES

R. Jones and R.J. Callinan

Structures Division, Aeronautical Research Laboratories,
Defence Science and Technology Organization, Victoria,
Australia

ABSTRACT

This paper develops a finite element method for determining the stress intensity factors along the edge of a crack in an arbitrary three-dimensional body. A special element is placed around the crack front and in each special element the stresses and displacements are derived using the asymptotic nature of the stress and displacement fields near a crack tip.

As illustrative examples the problems of a semicircular surface flaw and an internal penny shaped crack are first considered. In each case the computed values of the stress intensity factors are in excellent agreement with known analytical results. The repair of the surface flaw is then considered using a bonded overlay of composite material, and the effect of the overlay on the stress intensity factors is discussed.

KEYWORDS

Fracture mechanics, 3-D finite element methods, repair technology.

INTRODUCTION

This work forms part of a general research program into the repair of aircraft structures, using composite material, currently underway at the Aeronautical Research Laboratories, Australia, (Baker, 1978; Jones and Callinan, 1979, 1980). To date a large number of components have been repaired; these include wing skins, wing planks, and wheels. However, where as the previous studies have only been concerned in modelling the repair of cracks in thin metal sheets, the present paper is primarily concerned with the repair of surface flaws in thick structures.

We begin by developing a special crack tip element which may be used to obtain the stress intensity factors K_1,K_2 and K_3 along the edge of a crack in an arbitrary three-dimensional body. This element is then used to investigate the effect that a bonded overlay of composite material, covering a surface flaw, has upon the stress intensity factors along the edge of the flaw.

STRESS AND DISPLACEMENT FIELDS IN THE CRACK ELEMENT

Let us consider an elliptical flaw, see Figure 1, and define a system of x y z

co-ordinates such that the xoz plane lies in the plane of the crack and the y axis is directed perpendicular to this plane. If the semimajor and semiminor axes of the ellipse are of lengths a and b respectively then the equation of the crack front is given by

$$x^2/a^2 + z^2/b^2 = 1 \tag{1}$$

Let us also define a system of curvilinear co-ordinates, r,θ and φ such that

$$y = r \sin\theta,\quad x = a\cos\phi + r\cos\theta\cos\theta',\quad z = b\sin\phi + r\cos\theta\sin\theta' \tag{2}$$

where
$$\cos\theta' = b\cos\phi/\pi_0^{\frac{1}{2}},\quad \sin\theta' = a\sin\phi/\pi_0^{\frac{1}{2}} \tag{3}$$

and
$$\pi_0 = b^2\cos^2\phi + a\sin^2\phi \tag{4}$$

In the r,θ, and φ co-ordinate system, see Figure 1, all points on the crack front have r = 0 and the parametric equation of the crack is

$$x = a\cos\phi,\quad z = b\sin\phi \tag{5}$$

Let us now consider a special crack tip element which is bounded above by the plane $\phi = \phi_e$ (=constant) and below by the plane $\phi = \phi_{e+1}$ (=constant). The element is polygonal in planview and surrounds the crack front. This element is shown in Figure 2 for the special case when a = b. It is bounded by two planes both of which have y = const. and by two planes, which at the planes $\phi = \phi_e$ and $\phi = \phi_{e+1}$ have the same minimum distance from the crack front and which are perpendicular to the planes y = const. When a = b, as shown in Figure 2, the planes φ = const. pass through the origin but for a ≠ b they do not.

Within this element we will consider the stress and displacement fields to be given by the first term in their asymptotic expansions, see Sih and Liebowitz (1969).

$$\sigma_n = K_1\sigma_{1n} + K_2\sigma_{2n},\quad \sigma_t = K_1\sigma_{1t} + K_2\sigma_{2t},\quad \sigma_y = K_1\sigma_{1y} + K_2\sigma_{2y} \tag{6}$$

$$\tau_{ny} = K_1\tau_{1ny} + K_2\tau_{2ny},\quad \tau_{nt} = K_3\tau_{3nt},\quad \tau_{ty} = K_3\tau_{3ty} \tag{7}$$

$$\sigma_{1n} = \left(3\cos\frac{\theta}{2} + \cos\frac{5\theta}{2}\right)\Big/ 4\sqrt{2\pi r} \tag{8}$$

$$\sigma_{2n} = -\left(7\sin\frac{\theta}{2} + \sin\frac{5\theta}{2}\right)\Big/ 4\sqrt{2\pi r} \tag{9}$$

$$\sigma_{1t} = \frac{2\nu}{\sqrt{2\pi r}}\cos\frac{\theta}{2} \tag{10}$$

$$\sigma_{2t} = -\frac{2\nu}{\sqrt{2\pi r}}\sin\frac{\theta}{2} \tag{11}$$

$$\sigma_{1y} = -\frac{1}{4\sqrt{2\pi r}}\left(5\cos\frac{\theta}{2} - \cos\frac{5\theta}{2}\right) \tag{12}$$

$$\sigma_{2y} = -\frac{1}{4\sqrt{2\pi r}}\left(\sin\frac{\theta}{2} - \sin\frac{5\theta}{2}\right) \tag{13}$$

$$\tau_{3ty} = \frac{\cos\theta/2}{\sqrt{2\pi r}} \tag{14}$$

$$\tau_{3nt} = -\frac{\sin\theta/2}{\sqrt{2\pi r}}$$

$$\tau_{1ny} = \frac{1}{4\sqrt{2\pi r}}\left(\sin\frac{\theta}{2} - \sin\frac{5\theta}{2}\right) \tag{16}$$

$$\tau_{2ny} = \frac{1}{4\sqrt{2\pi r}}\left(3\cos\frac{\theta}{2} + \cos\frac{5\theta}{2}\right) \tag{17}$$

Here σ_{1t} is the coefficient of K_1 in the expression for σ_t, etc.

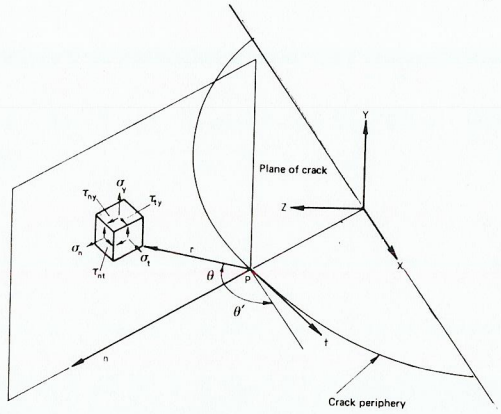

Figure 1. Stress components near periphery of crack, n and t are normal and tangential respectively to the periphery of the crack at P and lie in the crack plane.

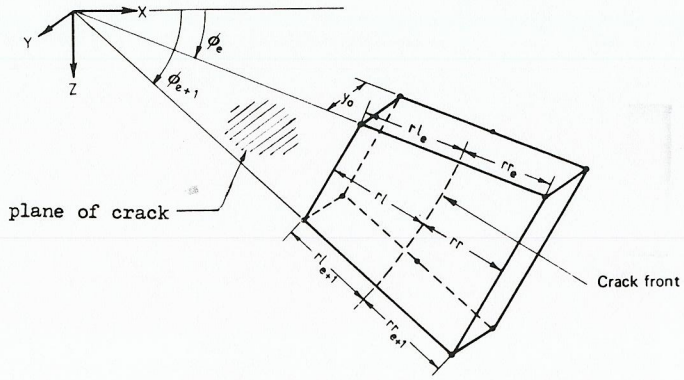

Figure 2. Geometry of the special element

In a similar fashion the displacements can also be expressed as

$$u_n = K_1 u_{1n} + K_2 u_{2n},\ u_t = K_3 u_{3t},\ u_y = K_1 u_{1y} + K_2 u_{2y} \tag{18}$$

where for exact details of the functions u_{1n}, u_{2n} etc. the reader is referred to Sih and Liebowitz (1969), page 149.

We now need to assume a functional form for the dependence of the stress intensity factors upon ϕ within the element. Perhaps the simplest, but by no means the only, such approach is to assume that K_1,K_2, and K_3 vary linearly within the element, i.e.

$$K_1(\phi) = K_{1e}\psi_1(\phi) + K_{1e+1}\psi_2(\phi) \tag{19}$$

with similar expressions for $K_2(\phi)$ and $K_3(\phi)$. Here

$$\psi_1(\phi) = 1 - \frac{(\phi - \phi_e)}{\phi_{e+1} - \phi_e},\ \psi_2(\phi) = \frac{\phi - \phi_e}{\phi_{e+1} - \phi_e} \tag{20}$$

This returns the values of K_{1e},K_{2e} and K_{3e} at the plane $\phi = \phi_e$ and the values of K_{1e+1}, K_{2e+1}, and K_{3e+1} at the plane $\phi = \phi_{e+1}$. Thus in addition to the degrees of freedom u_0,v_0,w_0,w_{xz},w_{yz},w_{xy} associated with rigid body motion the special element will have as degrees of freedom the values of K_{1e},K_{2e}, K_{3e},K_{1e+1},K_{2e+1}, K_{3e+1}. The vector λ,which contains these degrees of freedom,we define as

$$\lambda^T = K_{1e},K_{1e+1},K_{2e},K_{2e+1},K_{3e},K_{3e+1},u_0,v_0,w_0,w_{xy},w_{xz},w_{yz} \tag{21}$$

As shown by Jones and Callinan (1977) the "primitive" stiffness matrix K^e for this element may be obtained by differentiating the strain energy with respect to each of its elemental degrees of freedom. On carrying out this differentiation it is found that each element of the stiffness matrix is of the form

$$K_{ij} = \frac{1}{E}\int\int\int F_{ij}J dr d\theta d\phi \tag{22}$$

where E is Young's modulus, J is the Jacobian (= $r(\pi_o^{\frac{1}{2}} + r\cos\theta\ a\ b/\pi_o)$) and where for $i,j \leqslant 2$.

$$F_{ij} = \psi_i\psi_j\{(1-\nu^2)\ (\sigma_{1n} + \sigma_{1y})^2 + 2(1 + \nu)\ (\tau_{1ny}^2 - \sigma_{1n}\sigma_{1y})\}$$

for $i \leqslant 2,3 \leqslant j \leqslant 4$

$$F_{ij} = \tfrac{1}{2}\psi_i\psi_{j-2}\{2(1-\nu^2)\ (\sigma_{1n} + \sigma_{1y})\ (\sigma_{2n} + \sigma_{2y}) + 2(1+\nu)\ (2\tau_{1ny}\tau_{2y} - \sigma_{1n}\sigma_{2y} - \sigma_{2n}\sigma_{1y})\}$$

for $3 \leqslant i,j \leqslant 4$

$$F_{ij} = \psi_{i-2}\psi_{j-2}\{(1-\nu^2)\ (\sigma_{2n} + \sigma_{2y})^2 + 2(1+\nu)\ (\tau_{2ny}^2 - \sigma_{2n}\sigma_{2y})\}$$

for $5 \leqslant i,j \leqslant 6$

$$F_{ij} = \psi_{i-4}\psi_{j-4}^2(1+\nu)\{\tau_{3nt}^2 + \tau_{3ty}^2\} \tag{23}$$

and

$$F_{ji} = F_{ij} \tag{24}$$

for all values of i,j given above while for all other values of i.j, F_{ij} is zero. Here the triple integral is over the volume of the special element and is, in general, evaluated numerically.

So far we have primarily been concerned with determining the stiffness matrix for the element treating the vector λ as the vector containing the degrees of freedom of the element. However, in order to develop an element which is readily compatible with most finite element packages it is necessary to derive the stiffness matrix treating the nodal displacements, at each of the nodes of the element, as the basic degrees of freedom. This can be done using the procedure developed by Jones and Callinan (1977).

Let us define the displacements in the x,y, and z directions by u,v, and w respectively. If the special element is chosen to have m nodes then, at the ith node ($1 < i < m$) the cartesian displacements u_i,v_i, and w_i are related to u_n,u_y, and u_t by the formulae

$$u_i = u_n(r_i,\theta_i,\phi_i)\cos\theta_i' + u_t(r_i,\theta_i,\phi_i)\sin\theta_i' + u_o + z_i w_{xz} - y_i w_{xy} \tag{25}$$

$$v_i = u_y(r_i,\theta_i,\phi_i) + v_0 - z_i w_{zy} + x_i w_{xy} \tag{26}$$

$$w_i = u_n(r_i,\theta_i,\phi_i)\sin\theta_i' - u_t(r_i,\theta_i,\phi_i)\cos\theta_i' + w_0 + y_i w_{zy} - x_i w_{xz} \tag{27}$$

where r_i,θ_i,ϕ_i are the curvilinear co-ordinates of the ith node on the boundary of the special element and x_i,y_i, and z_i are the cartesian co-ordinates of this node. Substitution of the expressions for u_n,u_t, and u_y, as given by equation (18) into equations (25) (26) and (27) now results in a matrix equation of the form $L\underset{\sim}{\lambda} = \underset{\sim}{\delta}$

where $$\delta^T = u_1,v_1,w_1,u_2,v_2,w_2\ldots v_m,w_m \tag{28}$$

and L is a transformation matrix of dimensions 3m X 12. Since for the sake of accuracy, the special element will be coupled to the rest of the structure at more points than there are degrees of freedom we use the least squares technique to minimize the discontinuity of the displacements across the boundary of the special element. This procedure is described in detail by Jones and Callinan (1977) and gives

$$\underset{\sim}{\lambda} = (L^TL)^{-1}L^T\underset{\sim}{\delta} \tag{29}$$

so that when the nodal displacements u_i,v_i, and w_i are considered as the degrees of freedom then the element stiffness matrix becomes $((L^TL)^{-1}L^T)^T K (L^TL)^{-1}L^T$.

This formulation of the stiffness matrix may be used in conjunction with any of the standard finite element routines. When recovering the values of the stress intensity factors the procedure used by Blackburn and Helen (1977) which uses nodes on the crack face, coupled with the method of Chow and Lan (1976) which allows for a crack tip element of finite size, was used.

ILLUSTRATIVE EXAMPLES

As illustrative examples of this approach let us consider the following problems. An enclosed penny shaped crack, of radius 12.7 mm, located with its origin at the centre of a square bar of magnesium alloy, the length of the sides of the bar being 127 mm, and a semi-circular surface flaw of radius 12.7 mm centrally located in a rectangular bar of magnesium with dimensions 127 mm X 127 mm X 63.5 mm

(see Figure 3). In each case the bar is subject to a uniform tensile stress of 68.9 MPa. The Young's modulus of the block is 44.7 MPa and its Poisson ratio is 0.32.

In analysing the internal penny shaped flaw the symmetry conditions enabled us to model only one quarter of the bar. The mesh consisted of 278 nodal points with 198 elements and 3 special elements each of which is rectangular in plan view and has 10 nodal points. This mesh is shown in Figure 4. The value of the stress intensity factor K_1 at points A and B, as shown in Figure 3a, was found to be $K_1/\sigma\sqrt{a} = 1.17$ (cf. the value of 1.13 for an infinite body and the value of 1.15 allowing for a magnification of the previous value due to finite width effects). Here σ is the applied stress (= 68.9 MPa) and a is the radius of the crack (= 12.7 mm).

When analysing the semi-circular surface flaw problem use may also be made of the symmetry considerations so that the mesh used in the previous problem may also be utilized for the present problem.

The value of the stress intensity factor obtained at point B, the point of deepest penetration, was $K_1/\sigma\sqrt{a} = 1.19$ as against the theoretical value of 1.18 for a semi-circular surface flaw in a semi-infinite block and the value of 1.20 allowing for a magnification of this value due to back face effects. The value of the stress intensity factor obtained at point A, on the free surface, was $K_1/\sigma\sqrt{a} = 1.38$ as against the value of 1.39 for a semi-infinite block and the value of 1.41 allowing for a magnification due to finite width effects. In both cases the accuracy of the solution is sufficient for most engineering purposes and the error was never greater than 3%. Furthermore in the case of a through crack the analysis is similar to that given by Hilton (1973), and coincides with the analysis presented by Jones and Callinan (1977) in the case of a through crack in a thin sheet.

One very important fact, which should be stressed, is that for a part circular crack the volume integration in equation (22) simplifies to the extent that the r and θ integration may be carried out analytically. This leaves only the integration with respect to ϕ to be evaluated numerically. This simplification is due to the fact that for a part circular crack a = b, and

$$J = r(a + r\cos\theta),\ \theta' = \phi,\ \pi_0 = a^2 \qquad (30)$$

Full details of this simplified approach are given by Jones and Callinan (1978).

REPAIR OF SURFACE FLAWS

Let us now turn our attention to the repair of the surface flaw discussed above. Interest in this problem was generated by the boron fibre repair schemes developed at the Aeronautical Research Laboratories, Australia, for application to the Macchi landing wheel, see Baker (1978), and the repair scheme currently being developed, by the authors, for the main landing wheels of the Mirage IIIO. Both wheels develop fatigue cracks, the fatigue marking correlating quite well with the number of landings. In the case of the Macchi the wheels are usually discarded when the crack reaches a length of approximately 25 mm. The repair for the Macchi consists of two uniaxial boron epoxy laminate patches, the direction of the fibres being perpendicular to the crack, positioned so that both ends of the crack are covered (see Figure 5). This repair procedure is now the standard repair for the Macchi jet trainer in the Royal Australian Air Force and whereas without patching wheels tended to be rejected after about 60 landings, the repaired wheels last for at least 900 landings.

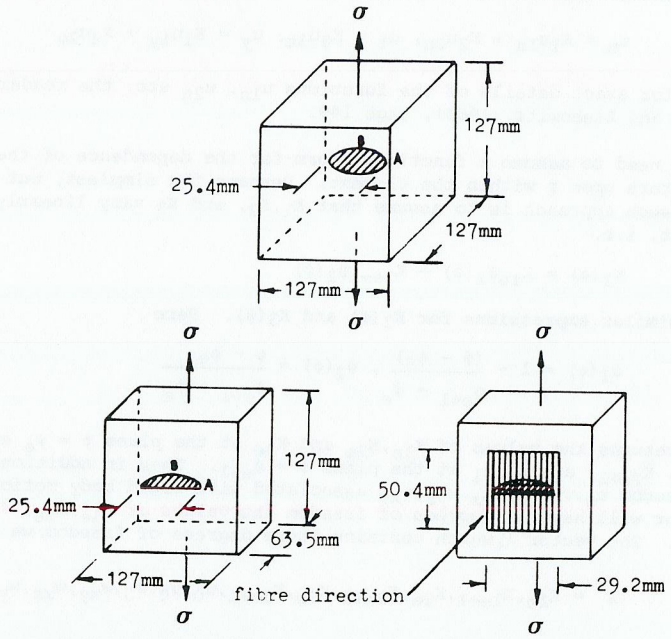

Figure 3. Geometry of the surface crack, the embedded penny shaped flaw, and the repair.

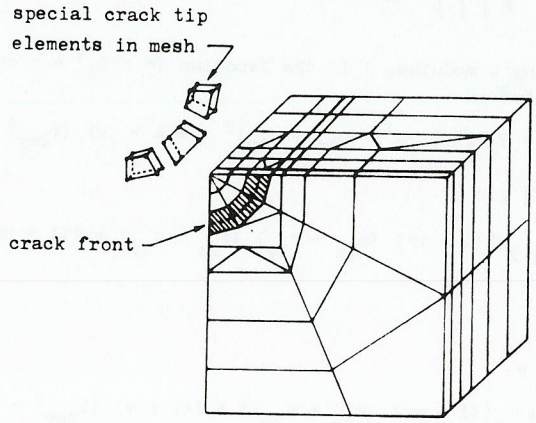

Figure 4. Finite element representation.

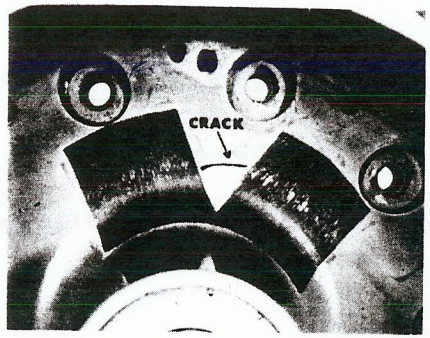

Figure 5. Repair to a Macchi wheel

Consider the surface flaw described in the previous section which is patched by a uniaxial boron-epoxy laminate of dimensions 50.4 mm X 29.2 mm the thickness of the patch being treated as a variable (see Figure 3(c)). The laminate moduli are as follows E_1 = 208.1 GPa, $E_2 = E_3$, E_1/E_2 = 8.18, $G_{12} = G_{13}$ = 7.24 GPa.
G_{23} = 4.94 GPa, $\gamma_{12} = \gamma_{13}$ = 0.1677, γ_{32} = 0.035

where the 1-axis is the fibre direction, the 2-axis is parallel to the crack, the 3-axis is in the thickness direction.

The patch is bonded to the magnesium alloy block by an adhesive, which is treated as being isotropic, with a shear modulus G_a of .965 GPa and a Poisson's ratio of 0.32.

This problem is an idealization of the actual repair, being developed by the authors, to be applied to the Mirage IIIO landing wheel in as much as the flaw in the wheel and the block have the same length at the surface. Both the block and the wheel are a magnesium alloy, the adhesive layer is the same thickness in both cases, and the actual repair will also be a uniaxial boron-epoxy laminate of approximately the same dimensions. As above the block is subjected to an applied uniform tensile stress. This is consistent with the state of stress in the wheel which, as determined by a detailed finite element analysis of the wheel, in the region of the flaw in an uncracked wheel, is predominently in tension with a very small bending field. The block was modelled as described, while the adhesive was modelled using 43 triangular prism elements and the composite was modelled using 86 triangular prism elements which have an orthotropic stress-strain law and which were based on the analysis presented by Barker and others (1972). The total number of nodal points involved was 381.

The results of this analysis are shown in Table 1 where the ratio of the stress intensity factors K_p/K_u, the fibre stress concentration at the crack σ_f/σ, the shear stress concentrations in the adhesive at the crack τ_c/σ and at the ends of the patch τ_e/σ are shown for various patch thicknesses. Here K_{1p} and K_{1u} are the values of the stress intensity factors after and before patching respectively.

TABLE 1 Repair of a Semi-Circular Flaw

Patch thickness (mm)	.508 mm	.762 mm	1.27 mm
Value of K_p/K_u			
(1) surface, A	.504	.459	.426
(2) bottom, B	.835	.804	.78
σ_f/σ	10.5	8.8	7.9
τ_c/σ	.829	.732	.70
τ_e/σ	.51	.65	.71

From this table we see that patches have a significant effect on the stress intensity factor at the crack-free surface intersection. However the stress intensity factor at point B, the deepest point, is much less effected by patching. We also see that at the crack the stress concentrations in both the fibre and the adhesive are very high. The high stress concentration in the fibres means that these repair schemes can be best used when the state of stress in the uncracked structure is relatively low. This is the case in the Mirage landing wheels where the cracking is primarily due to the presence of inclusions, typically 1 mm in diameter, and the high residual stress developed during the casting process. The high shear stress concentration in the adhesive at the ends of the patch is less important since as explained by Jones and Callinan (1980) this stress concentration can be removed by scarfing the patch.

Let us now turn our attention to the effect that different patch locations have upon the reduction in the stress intensity factor. This is an important problem since as can be seen from Figure 5, the geometry of the structure sometimes makes it difficult to cover the entire length of the crack so that a decision has to be made upon where to place the patches and how much of the crack needs to be covered. Table 2 shows the effect that placing two patches of dimensions 50.4 mm X 14.6 mm X 0.762 mm, each one of which is exactly half the size of the previous crack covering patch, at various distances from the centre of the flaw. The patches are placed symmetrically about the centre of the crack.

TABLE 2 Effect of Patch Location

distance of patch centre from centre of flaw	7.3 mm flaw completely covered	14.9 mm 40% of flaw covered	18.7 mm	21.3 mm
K_{1p}/K_{1u} (1) surface	.459	.526	.702	.916
(2) bottom	.804	.884	.933	.959

From Table 2 we see that although covering the entire length of the crack is best, when 40% of the crack has been covered a significant reduction in the stress intensity factor K_{1p} is achieved at the crack free surface intersection. As a

result it seems reasonable to recommend that a minimum of say 40-50% of the crack be covered.

So far we have primarily been concerned with a semi-circular surface flaw of radius 12.7 mm. We have seen that patching this flaw has relatively little effect on the stress intensity factor at B the point of deepest penetration. However it is reasonable to believe that for a semi-elliptical surface flaw, with the same length at the surface, the effect of a patch on the stress intensity factor at B increases as this point approaches the free surface, i.e. as the aspect ratio of the ellipse increases. This was partially confirmed by modelling the flaw in the block as a semi-elliptical surface flaw with a total surface length of 25.4 mm, as before, and a maximum penetration of 6.3 mm. (This shape of flaw closely resembles the flaw in the Mirage wheels). In this case the ratio of the stress intensity factors K_{1p}/K_{1u}, for a patch thickness of 0.762 mm, were found to be .40 at the free surface and .63 at the point of deepest penetration. This shows that for patched flaws increasing the aspect ratio of the flaw has a much more dramatic effect on the reduction of the stress intensity factor at the point of deepest penetration than it does on the reduction of the stress intensity factor at the surface.

CONCLUSION

In this study we first developed a simple finite element method for analysing flaws in a three dimensional body. The special element may be of any shape and for circular, or part circular flaws, requires only a limited use of numerical integration routines.

This element was then used to investigate the repair of surface flaws. The analysis revealed that patching these flaws with a bonded overlay of composite material was an effective method for reducing the stress field at the crack front. We also saw that for semi-elliptical surface flaws patching is far more effective for cracks of high aspect ratio (i.e. surface crack length/maximum penetration).

REFERENCES

Baker, A.A. (1978). Composites, 9, 11-16.

Barker, R.M., Fu-Tien Lin, Dana, J.R. (1972). Computers and Structures, 2, 1013-1029.

Blackburn, W.S., and Helen, T.K. (1977). Int. J. Numerical Methods in Engineering, II, 211-229.

Chow, G.L., and Lan, K.J. (1976). Int. J. Frac., 12, 488-490.

Hilton, P.D. (1973). Mechanics of Fracture, III, 273-297.

Jones, R., and Callinan, R.J. (1977). Int. J. Fracture, 13, 51-64.

Jones, R., and Callinan, R.J. (1978). Aeronautical Research Laboratories, Australia, Structures Report 374.

Jones, R., and Callinan, R.J. (1979). J. Struct. Mech., 7, 107-130.

Jones, R., and Callinan, R.J. (1980). Aeronautical Research Laboratories, Australia, Structures Report 376.

Sih, G.C. and Liebowitz, H. (1969). Fracture, Vol. 2, Academic Press, N.Y.